JOURNAL OF PROPULSION AND POWER
Vol. 14, No. 3, May–June 1998

Transport-Property Measurements in the Plume of an SPT-100 Hall Thruster

Lyon B. King,* Alec D. Gallimore,† and Colleen M. Marrese*
University of Michigan, Ann Arbor, Michigan 48109-2118

To understand the interaction between the SPT-100 thruster and the spacecraft, accurate knowledge of exhaust plume properties must be obtained. This investigation utilized a suite of interrelated diagnostic probes in an effort to provide detailed knowledge of the exhaust plume on a molecular kinetic level. Probes used for the investigation included a retarding potential analyzer, a planar Faraday probe, an emissive probe, both total- and radiant-heat-flux probes, as well as a newly developed neutral particle flux probe. Combining the knowledge gained from these probes it was possible to quantify the transport of mass, energy, and charge within the plume at 0.5- and 1.0-m radius from the thruster exit. Among the phenomena uncovered were a high-energy ionic annulus surrounding a narrow low-energy core within the plume at 0.5-m radius from the thruster exit. This core structure was filled in at 1.0-m radius. Additionally, a population of energetic charge-exchange neutrals was found within 25 deg of the thruster centerline along with the corresponding low-energy charge-exchange ions attributed to plume/background gas interactions.

Nomenclature

A_{probe} = area of retarding potential analyzer collector, m^2
C_r = relative interparticle speed, m/s
e = elementary charge, C
$F(V)$ = ion-energy distribution function, s/m
$f(u_i)$ = ion-velocity distribution function, s/m
I = current, A
j_i = ion-current density, A/m^2
K_1 = constant for calculating cross section, Eq. (8)
K_2 = constant for calculating cross section, Eq. (8)
k = Boltzmann constant
m_i = mass of ion, kg
m_n = mass of neutral, kg
n_i = density of ions, m^{-3}
n_m = measured density of neutrals, m^{-3}
n_n = density of fast neutrals, m^{-3}
P_{coll} = collision probability
P_m = measured pressure, Pa
q_{conv} = convective heat flux, W/m^2
s = path length traveled by particle, m
T_m = measured temperature of neutrals, K
T_p = temperature of probe surface, K
T_0 = temperature of slow neutrals, K
u_i = velocity of ions, m/s
u_m = velocity of measured neutrals, m/s
u_n = velocity of plume neutrals, m/s
V = probe voltage, V
$\langle x \rangle$ = average value of quantity x
$\boldsymbol{\lambda}$ = mean free path, m
σ_c = total cross section for charge exchange, m^2

Introduction

IN an effort to fully flight-qualify the SPT-100 for use in satellite missions, a great deal of research has focused on lifetime and performance issues of the thruster. As a result, the baseline operating conditions of the SPT-100 are now well established.[1] The next hurdle facing the widespread use of these devices is to develop an understanding of thruster/spacecraft interaction phenomena. The thruster may interact with the spacecraft through three fundamental processes: 1) thruster-generated electromagnetic interference (EMI), 2) particle impingement from the exhaust plume, and 3) radiant heating of spacecraft components. EMI may interfere with communication signals and instrument performance,[2] whereas particle impingement and radiant heating may cause physical damage to spacecraft hardware. This paper presents the results of a study to characterize the particle transport properties as well as the radiant heat environment produced by an SPT-100 plume.

The exhaust plume of an SPT-100 consists mainly of high-energy (200–300 eV) xenon ions produced and accelerated within the thruster. However, there are additional plume components owing to parasitic facility effects (during ground testing) and secondary ion processes occurring in the acceleration zone of the thruster. These additional components include slow propellant ions as well as both slow and fast neutral atoms.

The neutral and ionic portions of the plasma flow are linked through the process of resonant charge exchange (CEX). This process can occur within the thruster acceleration region as a result of entrained ambient background gas or un-ionized propellant, or it can occur downstream of the acceleration zone because of the ambient background gas. There are two approaches that can be used to detect CEX: One can either look for the slow ion products or detect the fast neutral products because their production rates are one-to-one.

The ionic portion of the plume, both high and low energy, can be detected in a straightforward manner through the use of classical electrostatic plasma probes. Previous studies have used such traditional techniques as Faraday probes, Langmuir probes, and retarding potential analyzers (RPAs)[3–5] to provide point measurements of the SPT-100 plume over a limited volume. The objective of this paper is to utilize the basic probes outlined in the preceding text in addition to new techniques over a larger volume of the SPT-100 plume than previously investigated. This paper reports the results of a study involving a broad array of traditional and innovative plasma probes. Emphasis has been placed on the interrelation of the probe data and the ability to derive secondary information regarding detailed plasma transport properties. In addition, results of a new

Received Jan. 25, 1997; revision received Dec. 10, 1997; accepted for publication Dec. 26, 1997.

*Graduate Student Researcher, Plasmadynamics and Electric Propulsion Laboratory, Department of Aerospace Engineering, 1919 Green Road, Room B107. Student Member AIAA.

†Assistant Professor, Plasmadynamics and Electric Propulsion Laboratory, Department of Aerospace Engineering, 1919 Green Road, Room B107. Senior Member AIAA.

probe developed to diagnose the neutral particle flux within the plasma are reported.

Description of Probes

Emissive Probe

Emissive probes were employed to measure plasma potentials that were required to correct ion-energy-distribution measurements. The probe filaments were tungsten wires that were 0.05 mm in diameter and approximately 6 mm long. Copper support wires were insulated from the plasma with alumina tubing.

Two methods were used to determine plasma potential. In the first method the filaments were heated to approximately 0.18 eV with a 60-Hz half-wave rectified sinusoidal current. The probe filament was biased with respect to ground through plasma potential with a 100-Hz triangular wave. The emission current of the probe was measured through a 1-kΩ shunt between the probe and ground. An oscilloscope was used to record the I–V characteristics during the first voltage ramp in the off segment of the heater cycle, ensuring that the filament was nearly a unipotential surface during measurements. This method is explained in greater detail by Kemp and Sellen.[6] In the second method the emissive probe was allowed to float in the plasma while the heater current was varied. Increasing the heater current drove the potential of the probe closer to the plasma potential at which further electron emission was retarded and the probe potential only varied slightly with an increasing heater current.[7] The results from both measurement methods were averaged to obtain the reported values.

Retarding Potential Analyzer

The most fundamental quantity from a gas-kinetic standpoint for any flow is the velocity distribution function of the flow constituents. This function when combined with the particle density can be theoretically used to calculate any flow property of interest.

For this investigation a gridded retarding potential analyzer (RPA) was used to determine the ion-energy distribution in the plume. This well-known technique uses a series of electrostatic grids upstream of a collecting surface to selectively repel plasma constituents. The RPA used in this investigation employed three grids. The first grid (and probe body) was allowed to float; thus minimizing probe disturbance to the plasma. The second grid was biased at a constant negative potential to repel all plasma electrons from the collector. The third grid was an ion-retarding grid connected to a variable high-voltage power supply. The potential of the ion-retarding grid is adjusted between 0 and 500 V to selectively repel ions from the collector.

An account of RPA operational theory can be found in most plasma-diagnostic texts.[8] Briefly, the potential of the ion-retarding grid is varied while monitoring the ion-current incident on the collector; thus data are obtained as $I(V)$ vs V. The negative derivative of these data is directly proportional to the ion-energy-distribution function $F(V)$, according to

$$-\frac{\mathrm{d}I}{\mathrm{d}V} = \frac{e^2 n_i A_{\text{probe}}}{m_i} F(V) \tag{1}$$

The probe body, grids, and collector were fashioned from stainless steel. The insulators between grids were made of Teflon® and ceramic. The entire probe was approximately 2.5 cm in diameter. The grid mesh sizes were as follows: floating grid, 0.112-mm-diam wire spaced at 0.266 mm on center; electron-retarding grid, 0.028-mm-diam wire spaced at 0.056 mm on center; and ion-retarding grid, 0.042-mm-diam wire spaced at 0.225 mm on center. For a more detailed description of the RPA used in this investigation refer to Ref. 9.

Faraday Probe

The Faraday probe was a 2.3-cm-diam planar disk spray-coated with tungsten. The tungsten was used to provide a very low secondary electron yield as a result of the impacting ions. This disk was mounted flush with the end of a stainless-steel cylindrical body. The probe body acted as a shield, ensuring a uniform electric field over the face of the collecting disk, eliminating edge effects. The collector and body of the Faraday probe were biased with a negative voltage of sufficient strength to repel all plasma electrons so that only ions were collected. The ion current collected by the Faraday probe provided a direct measure of the first moment of the ion-velocity distribution function, namely, ion-current density j_i. By combining this direct measurement of j_i with a known value of $\langle u_i \rangle$, the ion number density can be obtained as

$$n_i = j_i / e \langle u_i \rangle \tag{2}$$

Heat-Flux Probe

The convective heat flux, or power density, is related to the third moment of the particle velocity distribution function. For this investigation a heat-flux probe was designed based on commercially available transducers. The prevailing heat transfer mechanisms to the probe are identified as convective (kinetic) heating, radiant heating, ion-electron surface recombinative heating, electron current heating, and ablative cooling (sputtering). Among these phenomena, convective and radiant heating dominate the transport of energy because of the high exhaust velocity of the thruster in addition to the intense radiation produced by both the plasma and the hot thruster body. For ion-electron recombination heating, each ion deposits energy equal to the Xe^+ ionization energy (12 eV) to the surface as it recombines with an electron from the probe. Calculations show that this mode of probe heating comprises approximately 2% of the convective heating and is therefore ignored in this analysis. Elimination of electron current heating is achieved by biasing the probe to ground potential, which was found to be between 5 and 8 V lower than plasma potential (see Results section). Previous studies have measured the electron temperature to be close to 3 eV in the plume[3]; the grounded probe therefore collected negligible electron current. The ablative cooling is assumed to be insignificant in this model. Although comprehensive data for sputtering of surfaces exposed to 300 eV Xe^+ are not available, the kinetic and radiant heating of the hot plume are believed to be much larger than the ablative cooling.

The probe is shown in Fig. 1. The probe consisted of a water-cooled housing containing two identical Schmidt-Boelter heat-flux transducers placed 5 mm apart. The housing was instrumented with a thermocouple to provide a measurement of probe surface temperature. Each transducer was coated with optical black. One transducer was exposed directly to the environment to obtain a measure of total heat flux. The second identical transducer was covered by a sapphire window; this window shielded the device from convective heat flux. The useful transmission-wavelength range of sapphire is 200–5500

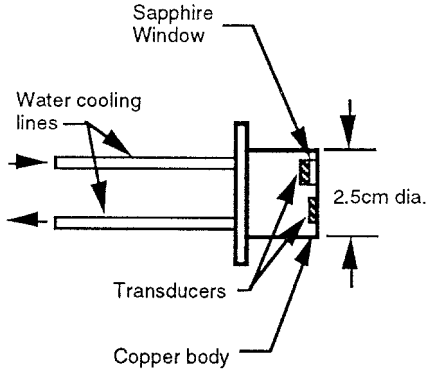

Fig. 1 Schematic of heat-flux probe showing both radiant- and total-heat-flux tranducers.

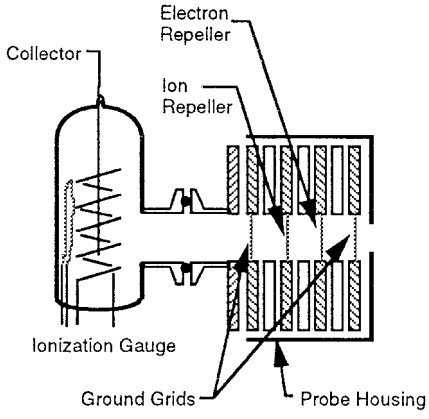

Fig. 2 Schematic of NPF probe showing grid arrangement and ionization gauge.

nm. Previous research has shown the plasma emissions in the SPT-100 plume to be confined mostly to 400–700 nm,[10,11] whereas the blackbody radiation from the hot thruster has an expected peak between 1000 and 5000 nm. It follows that the sapphire window is effectively transparent to the dominant forms of radiated energy within the plume and provides an effective measure of radiant heat flux. Calibration of these transducers, including the sapphire window configuration, was performed by the manufacturer to National Iinstitute of Standards and Technology-traceable standards over the heating and wavelength values expected in this test.

By subtracting the measured radiant heat flux from the measured total heat flux and approximating the heat transfer as outlined earlier, the particle convective heating can be calculated. Within this model the convective heat flux to such a probe is given as the difference between the incident plume heating and the reflected convective cooling, namely,

$$q_{\text{conv}} = n_i \left[\frac{1}{2} m_i \int_0^\infty u_i^3 f(u_i)\, \mathrm{d}u_i - 2kT_p \int_0^\infty u_i f(u_i)\, \mathrm{d}u_i \right] \quad (3)$$

It is apparent from Eq. 3 that a direct measurement of q_{conv} combined with known values for the first and third moments of the ion-velocity distribution function $f(u_i)$ and the probe body temperature T_p can be used to solve for the ion density n_i.

It is important to note that the heat-flux probe employs no retarding electrostatic fields, nor does it rely on charge-carrying particles for detection. Therefore, even though Eq. (3) is written solely in terms of ion properties, the measured convective heat flux is actually a result of both ions and neutral particles. It is possible (as will be shown in the Analysis and Discussion section) to calculate information about the neutral plasma component by comparing the heat-flux-derived ion density to the Faraday probe-derived ion density.

NPF Probe

In an attempt to characterize the neutral particle component of the plasma flow a new probe design was implemented. This probe is referred to as a neutral particle flux (NPF) probe. Detailed documentation of this design is presented elsewhere[12]; however, an overview of the probe operation will be presented here.

The probe is essentially a hybrid between an RPA and a vacuum-pressure gauge. A set of electrostatic grids are mounted to the inlet of a hot cathode ionization gauge tube. By using one grid as an electron-retarding grid and setting another grid to a high positive voltage to repel all ion flux from the tube, only the neutral component of the plasma is permitted to enter the tube. This neutral gas is ionized and sensed in the standard method of hot cathode ionization gauges. The gauge output is monitored on a standard hot cathode ionization gauge controller calibrated for Xe. A schematic of the NPF probe is shown in Fig. 2.

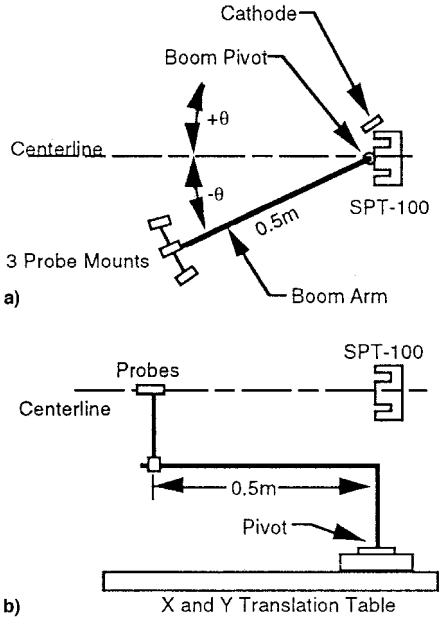

Fig. 3 Experimental setup showing boom/table/thruster layout and angle sign conventions: a) top and b) side views.

The pressure measured inside the ionization gauge tube is determined by the condition that the neutral particle flux entering the probe must be equal to the neutral particle flux exiting the probe. Specifically

$$n_n \langle u_n \rangle_{\text{in}} = n_m \langle u_m \rangle_{\text{out}} \quad (4)$$

In Eq. (4), quantities with a subscript n denote neutral particle properties within the plume, while quantities with a subscript m denote neutral particle properties within the measurement volume (gauge tube). Using free molecular theory to calculate the escape flux from the ion gauge tube yields

$$n_m \langle u_m \rangle_{\text{out}} = n_m \sqrt{kT_m / 2\pi m_n} \quad (5)$$

Utilizing the ideal-gas law to express n_m in terms of measured pressure P_m, and inserting this result into Eqs. (4) and (5) yields the relationship between probe-measured pressure and neutral particle flux into the probe

$$n_n \langle u_n \rangle_{\text{in}} = \frac{P_m}{\sqrt{2\pi m_n k T_m}} \quad (6)$$

It is apparent, then, that the pressure measured within the probe ionization gauge at a constant gauge temperature is directly proportional to the flux of neutral particles in the plume.

Experimental Setup

Facility

All tests were performed in the University of Michigan's Plasmadynamics and Electric Propulsion Laboratory (PEPL). The centerpiece of this laboratory is a large 6-m-diameter by 9-m-long vacuum chamber capable of base pressures of approximately 2.7×10^{-5} Pa at pumping speeds of over 25,000 l/s on xenon. A detailed description of this facility has been published previously.[13] Data were acquired and processed using a computerized digital data-acquisition system.

SPT-100

The thruster used for this experiment was a Fakel flight model SPT-100 Hall-effect thruster. The thruster was con-

trolled by a Space Systems/Loral power processing unit (PPU). Nominal operating conditions were utilized: discharge voltage = 300 V, discharge current = 4.5 A, and a total flow rate of 56 standard cubic centimeters per minute of Xe with a 7% cathode split. Tank pressure was maintained at less than 6×10^{-3} Pa true Xe pressure during all testing as determined by two hot-cathode ionization gauges.

Probes

The Faraday probe body, collector, and the RPA electron-retarding grid were biased approximately −30 V with respect to the thruster cathode potential. This voltage was sufficient to repel all plasma electrons while attracting only ion current.[3] The RPA ion-retarding grid was adjustable from 0 to approximately 500 V.

The heat-flux probe water-cooling lines were connected to a closed-loop thermostatically controlled refrigeration system. The probe body maintained a temperature of between 5 and 6°C for all test points.

The NPF probe electron-retarding grid was also set at −30 V with respect to thruster cathode potential. The ion-retarding grid of the NPF was set to a constant value of 500 V. This value, as determined from an RPA-type trace of probe output, was sufficient to repel all plume ions, admitting only neutral particles.[12]

Test Setup

For each test, three probes were mounted simultaneously to a rotating boom apparatus on a computerized remote-positioning system. An overview of the setup is shown in Fig. 3. The instruments were positioned 0.5 m from the boom pivot point. By positioning the pivot point directly beneath the thruster exit plane it was possible to obtain probe data at various angles off thruster centerline at a constant radial distance of 0.5 m by simply rotating the boom. As indicated in Fig. 3, positive angles off centerline indicate measurements taken on the cathode side of the thruster, while negative angles denote the noncathode half-plane. This convention will be followed throughout the paper. By translating the pivot point of the instrument boom in addition to rotation, data were collected at radial positions of 1.0 m from the thruster exit plane while ensuring that the probes remained normal to the flow. Angular resolution of the traversing mechanism is better than 0.1 deg; however, initial alignment of the probes with the zero point (thruster axis) could only be confidently performed to within 3 deg. The relative uncertainty in angular position between data points is thus 0.1 deg, but the 3-deg absolute offset has been conservatively indicated as an error bar for all data points.

Upon completion of the baseline data sets the Faraday probe configuration was changed: the Faraday probe was turned backward to quantify the background ambient plasma conditions separately from the direct plume flux. In this position the collecting surface of the probe remained at 0.5-m radius from boom pivot point; however, the probe faced directly away from the thruster. This allowed the probe body to shield the collecting surface from the direct plume flux, creating a quiescent wake. By sampling the ion-current flux within this wake it was possible to directly measure the ambient background plasma conditions caused by chamber pumping limitations and CEX.

Results

Emissive Probe

Plasma potential measurements were taken in the negative half-plane of the thruster plume between 0 and −60 deg off centerline at both 0.5- and 1.0-m radial distance. At 0.5-m measurements were taken every 15 deg, while the 1.0-m data set includes measurements every 10 deg. The plasma potential varied between 7.2 and 5.4 V with respect to tank ground, while the thruster cathode remained at a constant −22 V with respect to tank ground. These measurements are shown in Fig. 4.

RPA

RPA data were collected in the negative half-plane (noncathode side) of the thruster from centerline out to −60 deg. Beyond 60 deg off-axis the collected current fell to levels for which the numerical differentiation required for data reduction produced unacceptably large error-to-measurement ratios. Thus, all successive probe data were limited to points for which RPA traces were available. For the 0.5-m data set, sweeps of ion current vs retarding voltage were recorded every 5 deg, with sweeps every 10 deg for the 1.0-m data. Peak ion-current values were in the range of tens of μA near centerline down to hundreds of nA far off centerline for both 0.5- and 1.0-m sweeps. Examples of these sweeps are shown as Fig. 5 for the 0.5-m data set. The 10% measurement error represents uncertainties in the collected current. These uncertainties were then propagated through all plume analyses incorporating integrated values based on RPA measurements.

Faraday Probe

Ion-current density was measured in the full plane both at 0.5- and 1.0-m radius from −60 to 60 deg at 5-deg increments. The centerline-plume ion-current density fell from 5 mA/cm^2 at 0.5 m to about 1.6 mA/cm^2 at 1.0 m. The background wake ion-current flux showed similar trends; however, the current values were two orders of magnitude lower than the corresponding ram flux. The Faraday probe data are shown in Fig. 6. The indicated 10% error is because of uncertainties in the measured current and probe collection area.

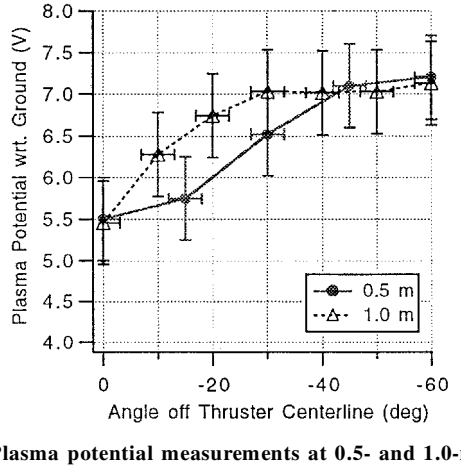

Fig. 4 Plasma potential measurements at 0.5- and 1.0-m radius from thruster.

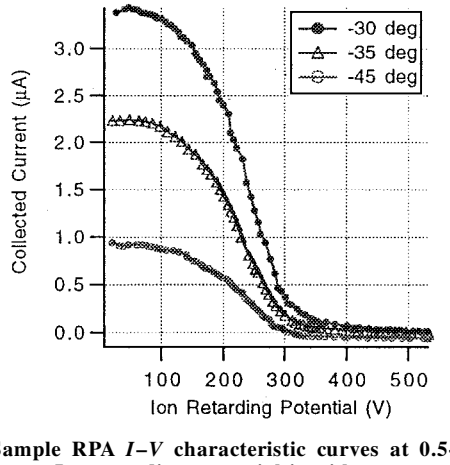

Fig. 5 Sample RPA *I–V* characteristic curves at 0.5-m radius from thruster. Ion-retarding potential is with respect to thruster cathode. Uncertainty in current is less than 10%.

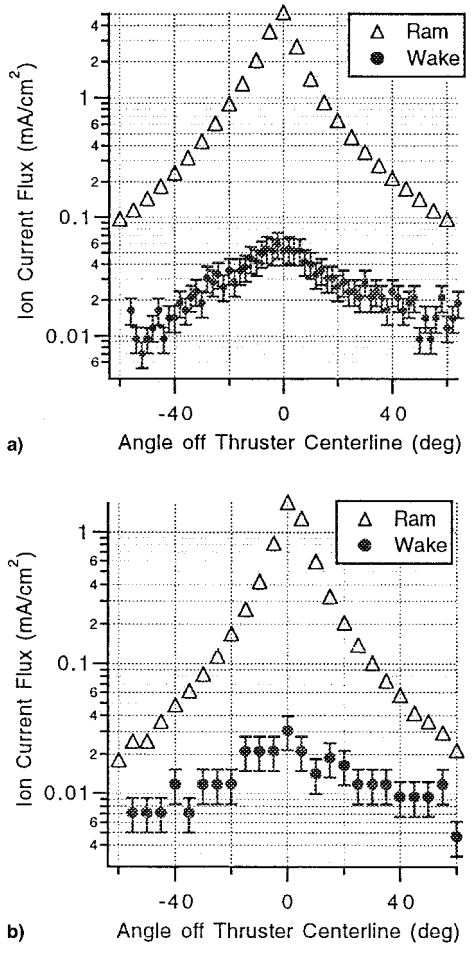

Fig. 6 Ram and wake ion-current density at a) 0.5- and b) 1.0-m radius from thruster exit. Uncertainty in angular position is 3 deg, uncertainty in ram current flux is less than 10%.

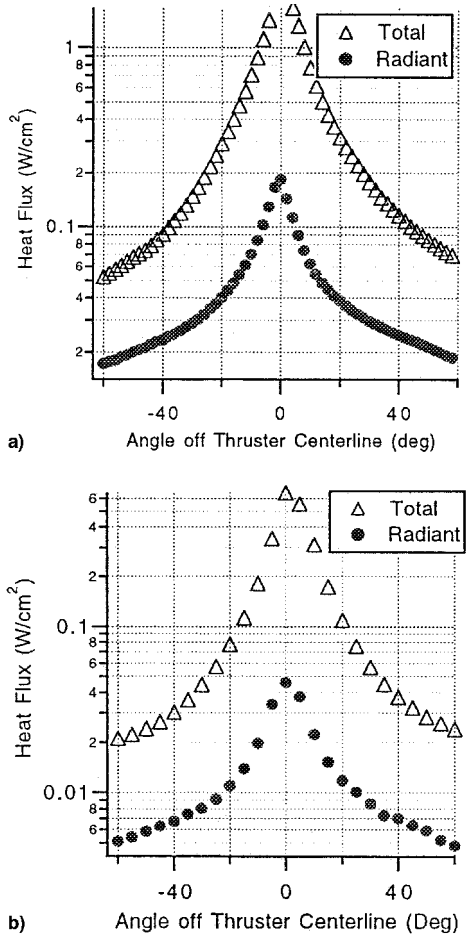

Fig. 7 Radiant- and total-heat-flux measurements at a) 0.5- and b) 1.0-m radius from thruster exit. Uncertainty in heat flux less than 10%, uncertainty in angular position is 3 deg.

Heat-Flux Probe

Data were obtained with the heat-flux probe at 2-deg increments from −60 to 60 deg at 0.5-m radius from the thruster exit and 5-deg increments at 1.0 m. For the positions of −2, 0, and 2 deg at 0.5 m, the measured total heat flux exceeded the calibrated range of the sensor. Total heat-flux data are therefore unavailable for these points. The radiant- and total heat-flux data are shown in Fig. 7. Because of plasma sputtering the surface texture and, therefore, the transmission properties of the sapphire window are expected to change over time. However, the entire data set reported in Fig. 7 required the heat-flux probe to be exposed to the plasma for less than 60 s. Over this short period no appreciable variation in the window surface was expected; posttest visual inspection confirmed the absence of window damage. The 10% error indicated in Fig. 7 represents uncertainties in calibration as reported by the transducer manufacturer over the measurement range of interest, with an additional 2% error to reflect neglect of ion–electron surface recombinative heating.

NPF Probe

The NPF probe data were obtained at 2-deg increments in the half-plane from −60 to 0 deg at 0.5 m and at 5-deg increments at 1.0 m. The overpressure protect set point for the hot-cathode tube was set for 0.8 Pa. Above this pressure, the tube de-energized to prevent damage to the filament. Because of this, data within 10 deg of centerline could not be obtained at either 0.5 or 1.0 m. The NPF probe data are shown in Fig. 8. Error bars reflect uncertainty in the calibration of the total pressure gauge as supplied by the manufacturer.

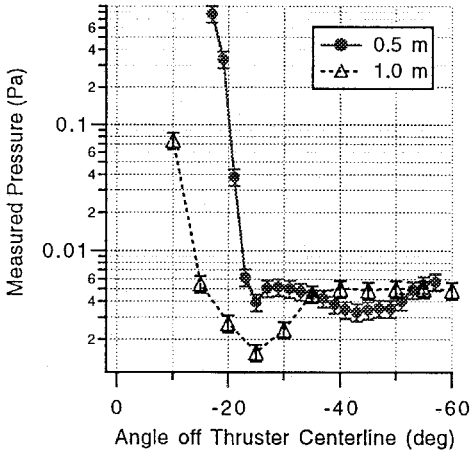

Fig. 8 Measured pressure inside NPF gauge tube at 0.5- and 1.0-m radius. Uncertainty in angular position is 3 deg.

Analysis and Discussion

Ion-Energy Distribution

As shown in Eq. (1), the nonnormalized ion-energy distribution can be obtained by numerically differentiating the $I(V)$ vs V data sweeps of the RPA. Although the values of A_{probe} and n_i are required to find $F(V)$ via Eq. (1), differentiation of the raw data provides a curve that is directly proportional to $F(V)$. This curve can then be normalized such that the total area under the curve is unity providing a direct calculation of $F(V)$ independent of the constants A_{probe} and n_i. To ensure the ac-

curacy of the ion-energy distribution a discrete but important correction must be applied to the RPA data: although the first grid and probe body were allowed to float, the ion energy is recorded in volts with respect to thruster cathode potential. This induces an energy shift to the ions as they fall from plasma potential to reference cathode potential. The cathode potential was monitored and found to be approximately −22 V with respect to tank ground. As can be seen from the plasma potential data of Fig. 4, this imposes an appreciable energy shift to the ions (on the order of 30 V) that must be accounted for during postprocessing.

The entire data set of ion-energy distribution curves is not included in the present paper; however, the dominant trends are evident in the sample data of Fig. 9. For angles near thruster centerline, the ion-energy distribution is sharply peaked near a most probable energy of around 230 V, with a full-width-at-half-max (fwhm) of 100 V at −30 deg off centerline. For larger angles the distribution becomes much broader because of the appearance of a population of lower energy ions. Although the most probable ion energy remains 230 V, the fwhm is increased to more than 150 V at −45 deg. This broadening of the energy distribution for large angles was evident in all data points for both 0.5- and 1.0-m data sets; however, the most probable ion energy remains very near 230 V for each trace. Although the thruster discharge voltage was 300 V, a high-energy tail of ions with energies greater than the discharge voltage was found in all RPA traces. The size of this tail was largest for angles near thruster centerline and decreased with increasing angle. Furthermore, the tail was smaller in the 1.0-m data sets than for corresponding angles in the 0.5-m data. Although the existence of this tail has been documented by other researchers,[14] a precise explanation for its origin remains unclear.

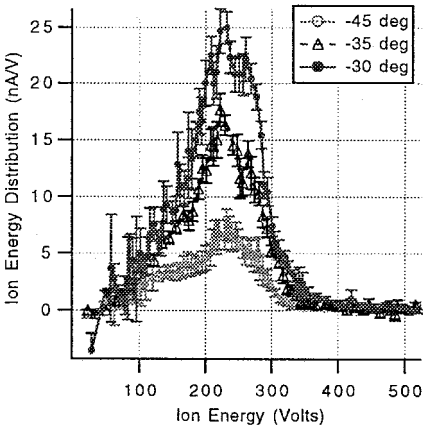

Fig. 9 Sample of nonnormalized ion-energy distribution curves at 0.5-m radius from thruster exit. Ion energy is with respect to thruster cathode.

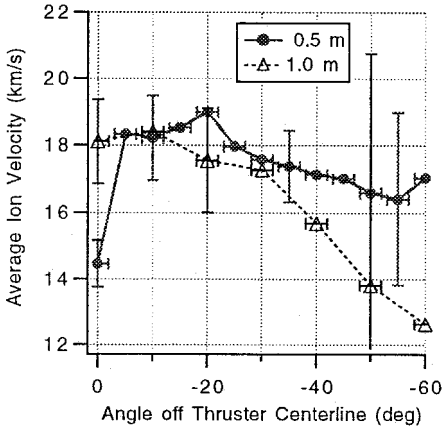

Fig. 10 Average ion velocity based on RPA data at 0.5- and 1.0-m radius. Sample error bars included to indicate magnitude of uncertainty caused by propagated errors.

Quantitatively, the ion-energy distribution curves can be better understood by numerically evaluating the first few moments. Previous research has shown the plume of the SPT-100 to be comprised almost entirely of singly ionized Xe.[10] Utilizing this assumption, it is trivial to convert the $F(V)$ to $f(u_i)$. The moments of these velocity distributions can then be evaluated and utilized to calculate ionic transport properties. The first moment, or average ion velocity, was computed numerically and is shown in Fig. 10 for both 0.5- and 1.0-m radius. The error bars of Fig. 10 represent the propagation of original measurement uncertainties through the numerical integration.

A striking result of this analysis was the discovery of a very narrow low-energy core surrounded by a slightly higher-energy annulus with a peak at −20 deg in the plume at 0.5-m radius from thruster exit. Although such a topology would be expected in the near field of the thruster because of the annular shape of the discharge chamber, it was believed that the divergence of the ion beam would smear out this configuration very rapidly. On the contrary, the average ion velocity on centerline at 0.5 m is less than the velocity computed for any other point measured in the 0.5-m data set. This low-energy core is very narrow, limited to a region in space with a half-angle of 5 deg about thruster centerline. It should be noted, however, that this annulus structure was not uncovered in the Faraday probe data. Because the Faraday probe measures $en\langle u_i\rangle$, the rapidly increasing ion density near centerline overwhelms the dip in $\langle u_i\rangle$ and a monotonically increasing ion-current density results. The high-energy annulus/low-energy core structure is not present in the 1.0-m data set. At this downstream location the beam divergence has completely filled in the core. In addition to the smearing of the spatial energy structure, the ion velocity for large angles (greater than 30 deg) is much less at 1.0 m than at 0.5 m.

The existence of a high-energy plasma annulus with low spatial divergence is consistent with thruster discharge chamber geometry and field topology. The high-energy ions are formed closer to the anode and, hence, farther back inside the discharge chamber. These ions, to escape the discharge chamber without colliding with the wall, must have their velocity vectors geometrically contained within a defined solid angle. Those ions formed near the end of the discharge chamber farther from the anode will have lower energy as a consequence of the field topology, and will also have their velocity vectors distributed about a larger allowed solid angle.

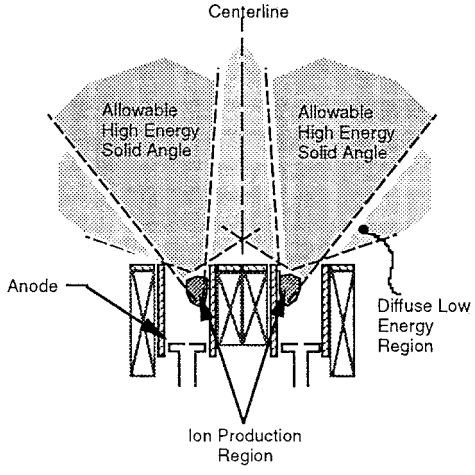

Fig. 11 Schematic representation of mechanism causing high-energy annulus and low-energy core in thruster plume. Ion production region denoted as according to Bishaev and Kim.[15] High-energy ions are formed closest to anode.

The low-energy core in the mid-to-near field is most likely a result of the distribution of ion production within the discharge chamber. According to data obtained by Bishaev and Kim,[15] the majority of the ionization within the thruster occurs very near the inner wall of the discharge chamber. For these ions to escape the discharge chamber without colliding with a wall and being neutralized, their velocity vectors must be directed largely away from thruster centerline. Such a distribution of velocity vectors would produce a depletion of high-energy ions on thruster centerline until a considerable distance downstream. Such a scenario is depicted conceptually in Fig. 11, with the high-ion-formation region of Bishaev and Kim indicated.

Density Distribution

With the broad interrelated suite of data obtained in this study, it was possible to calculate two measures of particle density. In the first method, the Faraday probe-measured j_i is combined with the first moment of the ion velocity distribution function $\langle u_i \rangle$ and used to predict the ion density according to Eq. (2). The second method is based on the heat-flux-probe data: by subtracting the measured radiant heat flux from the measured total heat flux, the value of particle convective heating q_{conv} is obtained. Combining q_{conv} with numerically calculated values of $\langle u_i \rangle$ and $\langle u_i^3 \rangle$, and recalling that the heat-flux probe is sensitive to both neutrals and ions, the total particle density (ion and neutral) can be calculated according to Eq. (3).

Based on the methods outlined previously, two separate values of particle density are presented in Fig. 12 for the 0.5-m data, and Fig. 13 for the 1.0-m data. The error bars in Figs. 12 and 13 represent the propagation of all original measurement uncertainties. As can be seen in the figures, both methods of calculating particle density produce comparable results indicating that neutrals represent only a small fraction of the flow. The maximum difference between the values at 0.5 m is approximately 25% at −5 deg, with a somewhat larger discrepancy of 40% on centerline at 1.0 m.

Neutral Particle Properties

The neutral component of the plume was evaluated in this investigation using two methods: 1) direct measurement of neutral particle flux using the NPF probe, and 2) calculation of neutral particle properties based on the interrelation of other probe data. The measured neutral pressure within the NPF probe displayed as Fig. 8 can be converted via Eq. (6) to provide a measure of neutral particle flux. This quantity is plotted in Fig. 14 for both the 0.5- and 1.0-m data sets. The NPF data suggest a region of high neutral particle flux near plume centerline. Although the data sets are limited to angles larger than 10 deg, it is evident that a well-defined core of neutral particles is present in the plume. This core is surrounded by a region of depressed neutral flux bottoming out at about −25 deg, followed by a subsequent rise to ambient background pressure outside of about −40 deg. The region of depleted neutrals near −25 deg corresponds loosely with the high-energy ionic annulus shown in Fig. 10 at 0.5 m. The relationship between the depressed neutral flux and elevated ion energy is not fully understood at this writing.

The second method of determining neutral properties stems from the inherent difference between the Faraday probe and the heat-flux probe. By subtracting values calculated on the basis of Faraday data from values calculated from the heat flux data, it is possible to quantify the contribution of the neutral

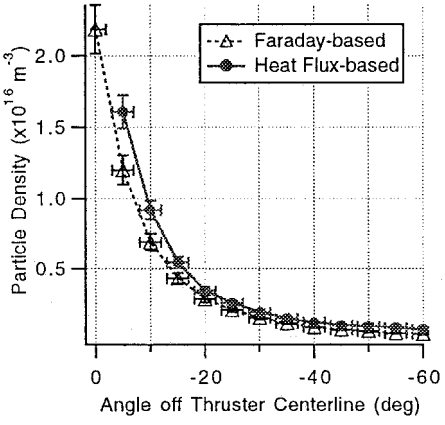

Fig. 12 Comparison of calculated particle density based on heat-flux probe and Faraday probe at 0.5-m radius from thruster.

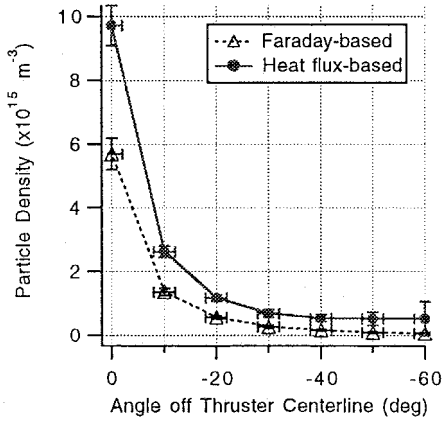

Fig. 13 Comparison of calculated particle density based on heat-flux probe and Faraday probe at 1.0-m radius from thruster.

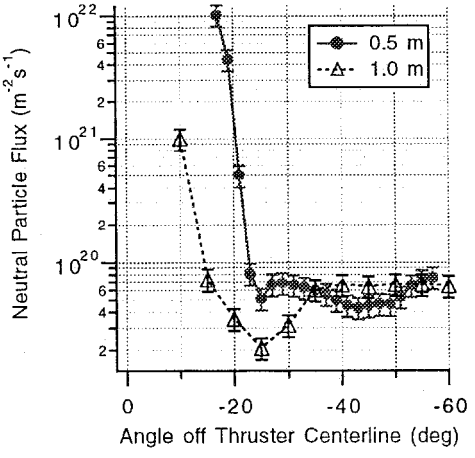

Fig. 14 Measured neutral particle flux at 0.5- and 1.0-m radius.

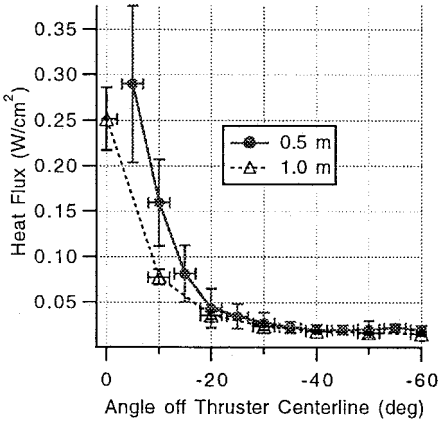

Fig. 15 Calculated neutral particle convective heating at 0.5- and 1.0-m radius.

flow. This method was used to evaluate the neutral particle heat flux. The value of convective heat flux because of both neutrals and ions was calculated by subtracting the measured radiant heat flux from the measured total heat flux. The ionic contribution to the convective heat flux was derived according to Eq. (3) with the ion density calculated from the Faraday probe data via Eq. (2). Subtracting the derived ionic heat flux from the measured convective (ion and neutral) heat flux yields the value of neutral particle heating. This quantity is plotted in Fig. 15 for both 0.5- and 1.0-m data sets, with error bars representing the propagation of all measurement uncertainties. As expected, the neutral particle heating is greater at 0.5 m than at 1.0 m. Furthermore, the neutral heating is confined to a region within 25 deg of thruster centerline falling off to negligible values sharply for larger angles. This corroborates the NPF data that also showed the neutral flux to be contained within a well-defined region with a half-angle of 25 deg.

CEX Processes

As stated in the Introduction, CEX processes can be evaluated either by quantifying the slow ion products or the fast neutral products because their production rates are one-to-one. In this investigation both methods of detecting CEX products were attempted.

Analysis of the neutral component of the plasma is missing one vital piece of information to close the CEX analysis: the value of the neutral particle velocity distribution function. However, some insight to the neutral component can be derived from available quantities. From a top-level perspective, it would be valuable to know whether the neutrals detected by the NPF are slow ambient background particles, or fast CEX products. If we assume that the neutrals are slow, macroscopically stagnant Maxwellian particles at temperature T_0, then the free molecular convective heating to the water cooled probe is computed as

$$q_{\text{conv}} = \tfrac{1}{4} n_n \langle u_n \rangle k (T_n - T_p) \tag{7}$$

Because the flow has been assumed to be stagnant, the pressure measured by the NPF probe would be the true ambient neutral pressure; this could be converted via the ideal gas law to obtain n_n. Evaluating Eq. (7) for the sample point at -15 deg from centerline at 0.5 m, where $P_m = 0.8$ Pa (from Fig. 8), and assuming a neutral background temperature $T_n = 300$ K yields a value of neutral particle convective heating of 3.2×10^{-4} W/cm^2. This is 250 times lower than the value of 0.08 W/cm^2 obtained from the data for the neutral heating at this location (see Fig. 15). Even if the assumed background neutral temperature is increased to agree with the data-obtained heating, the neutrals would have to have an unrealistically high temperature of over 100,000 K at this sample point to account for the 0.08 W/cm^2 measured neutral heating. It is apparent that a distribution of slow neutrals cannot account for the measured neutral convective heating and that the neutrals measured with the NPF probe are most likely highly energetic CEX products.

The appearance of CEX products is supported by a statistical collision analysis of the plume/background gas interaction. The charge exchange collision cross section for Xe^+–Xe can be computed according to[16]

$$\sigma_c = (K_1 \ell n\, C_r + K_2)^2 \times 10^{-20}\ \text{m}^2 \tag{8}$$

with $K_1 = -0.8821$ and $K_2 = 15.1262$. For this investigation, with an average relative interparticle speed $C_r = 17$ km/s and a tank background pressure of 6×10^{-3} Pa, the CEX mean free path is approximately 1.5 m. Although this mean free path is longer than the largest path length in this investigation (1.0 m), examination of the collision statistics reveals that the effect of CEX is not negligible. The fraction of particles that undergo a collision within a path length s is given by the well-known survival equation as

$$P_{\text{coll}}(s) = (1 - e^{-s/\lambda}) \tag{9}$$

Equation (9) shows that at 0.5 m from the thruster exit, almost 30% of the emitted plume ions have suffered a CEX collision; this increases to a value of almost 50% of the ions undergoing a CEX collision by 1.0 m. In reality, the tank background pressure of 6×10^{-3} Pa is not composed entirely of neutral Xe. Because of facility base-pressure limitations, a portion of this background pressure is residual air. Although accounting for this lower background Xe density would increase the computed Xe^+–Xe mean free path, other nonresonant collisions between particles of dissimilar masses must be accounted for; these collisions would likely affect the plume ions similarly to the ideal case considered here.

Conclusions

By making comprehensive measurements of related ion and neutral-particle properties within the plume, it was possible to gain insight into plume structure and thruster operation. The phenomena investigated included ion-neutral charge-exchange, spatial distribution of ion energy within the plume, and information regarding beam and ambient plasma properties.

Analysis revealed that the plume possesses a very narrow low-energy core surrounded by an annulus of slightly higher energy at 0.5-m radius from the thruster exit. This core is filled in by beam divergence at 1.0 m. This structure is consistent with thruster discharge chamber geometry, field topology, and distribution of ion production.

Through the use of a new probe design coupled with heat-flux measurements, it was possible to derive information regarding neutral particle properties within the plume. The data analysis suggests that these neutral particles are the high-energy products of ion-neutral CEX collisions. Furthermore, these high-energy neutrals are contained almost entirely within a cone with a half-angle of 25 deg off thruster centerline. It is apparent that facility-induced interactions between background gas and plume ions are not negligible even at mPa tank pressures.

Acknowledgments

The research reported herein was sponsored by the U.S. Air Force Office of Scientific Research. Mitat Birkan was the contract monitor, this support is gratefully acknowledged. The authors would also like to thank Michael Day of Space Systems/Loral for use of the SPT-100 and PPU, instrument fabricator Terry Larrow, and PEPL researchers Matt Domonkos, John Foster, James Haas, and Sang-Wook Kim.

References

[1]Garner, C. E., Brophy, J. R., Polk, J. E., and Pless, L. C., "A 5,730-Hr Cyclic Endurance Test of the SPT-100," AIAA Paper 95-2667, July 1995.

[2]Ohler, S., Gilchrist, B., and Gallimore, A., "Microwave Plume Measurements of an SPT-100 Using Xenon and a Laboratory Model SPT Using Krypton," AIAA Paper 95-2931, July 1995.

[3]Myers, R. M., and Manzella, D. H., "Stationary Plasma Thruster Plume Characteristics," *Proceedings of the 23rd International Electric Propulsion Conference*, Vol. 2, 1993, pp. 893–912.

[4]Manzella, D. H., and Sankovic, J. M., "Hall Thruster Ion Beam Characterization," AIAA Paper 95-2927, July 1995.

[5]Pencil, E. J., Randolph, T., and Manzella, D. H., "End-of-Life Stationary Plasma Thruster Far-Field Plume Characterization," AIAA Paper 96-2709, July 1996.

[6]Kemp, R. F., and Sellen, J. M., Jr., "Plasma Potential Measurements by Electrons and Emissive Probes," *Review of Scientific Instruments*, Vol. 37, No. 4, 1996, pp. 455–461.

[7]Hershkowitz, N., "How Langmuir Probes Work," *Plasma Diagnostics: Discharge Parameters and Chemistry*, edited by O. Auciello

and D. Flamm, Vol. 1, Academic, San Diego, CA, 1989.

[8]Hutchinson, I. H., *Principles of Plasma Diagnostics*, Cambridge Univ. Press, New York, 1987.

[9]Marrese, C. M., Gallimore, A. D., Haas, J., Foster, J. E., King, L. B., and Kim, S. W., "An Investigation of Stationary Plasma Thruster Performance with Krypton Propellant," AIAA Paper 95-2932, July 1995.

[10]Manzella, D. H., "Stationary Plasma Thruster Plume Emissions," *Proceedings of the 23rd International Electric Propulsion Conference*, Vol. 2, 1993, pp. 913–923.

[11]Leray, P., Bonnet, J., and Pigache, D., "Spatially Resolved Emission Spectroscopy Along a SPT Channel. Interpretation of Data by Collisional-Radiative Model," Proceedings of the 25th International Electric Propulsion Conference, 1997.

[12]King, L. B., and Gallimore, A. D., "A Gridded Retarding Pressure Sensor for Ion and Neutral Particle Analysis in Flowing Plasmas," *Review of Scientific Instruments*, Vol. 68, No. 2, 1997, pp. 1183–1188.

[13]Gallimore, A. D., Kim, S. W., Foster, J. E., King, L. B., and Gulczinski, F.S., III, "Near- and Far-Field Plume Studies of a 1 kW Arcjet," *Journal of Propulsion and Power*, Vol. 12, No. 1, 1996, pp. 105–111.

[14]Burgrova, A. I., Desyatskov, A. V., and Kharchevnikov, V. K., "Experimental Determination of Ion Energy at the Outlet of SPT-ATON," *Proceedings of the 24th International Electric Propulsion Conference*, Vol. 1, pp. 364, 365.

[15]Bishaev, A. M., and Kim, V., "Local Plasma Properties in a Hall-Current Accelerator with an Extended Acceleration Zone," *Soviet Physics—Technical Physics*, Vol. 23, No. 9, Sept. 1978, pp. 1055–1057.

[16]Rapp, D., and Francis, W. E., "Charge Exchange Between Gaseous Ions and Atoms," *Journal of Chemical Physics*, Vol. 37, No. 11, 1962, pp. 2631–2645.